4 Undrained Cylindrical Cavity Expansion in a Cam-Clay Medium

4.1 Problem Statement

The stress and pore pressure changes due to the expansion of a pressuremeter in a saturated clay mass are analyzed using the model of a cylindrical cavity in an infinite Cam-clay medium. The effect of the finite length of the measuring device is not considered.

In the experiment, the radius a of the cavity is expanded to up to twice its original size, a_0. The properties of the Cam-clay material, which correspond to a Boston Blue Clay, are (Carter et al. 1979)

undrained cohesion (C_u)	1 MPa
shear modulus (G)	$74 \times C_u$
soil constant (M)	1.2
slope of normal consolidation line (λ)	0.15
slope of elastic swelling line (κ)	0.03
reference pressure (p'_1)	C_u
specific volume at reference pressure (v_λ)	2.3
density (ρ)	10^3 kg/m^3

The clay is normally consolidated with in-situ stresses, $\sigma'_r = \sigma'_\theta = -1.65C_u$, $\sigma'_z = -3C_u$, and initial excess pore pressure, $u_e = 0$. The shear modulus of the material is assumed to remain constant during the simulation. The pressuremeter membrane is considered impermeable, and the fluid bulk modulus is much larger than that of the soil, so that the numerical simulation can be carried out under undrained conditions.

4.2 Modeling Procedure

The problem is modeled using an axisymmetric configuration and plane-strain boundary conditions, as represented in Figure 4.1. The *FLAC* model is of finite extent, but the length, L, is chosen as very large compared to a_0.

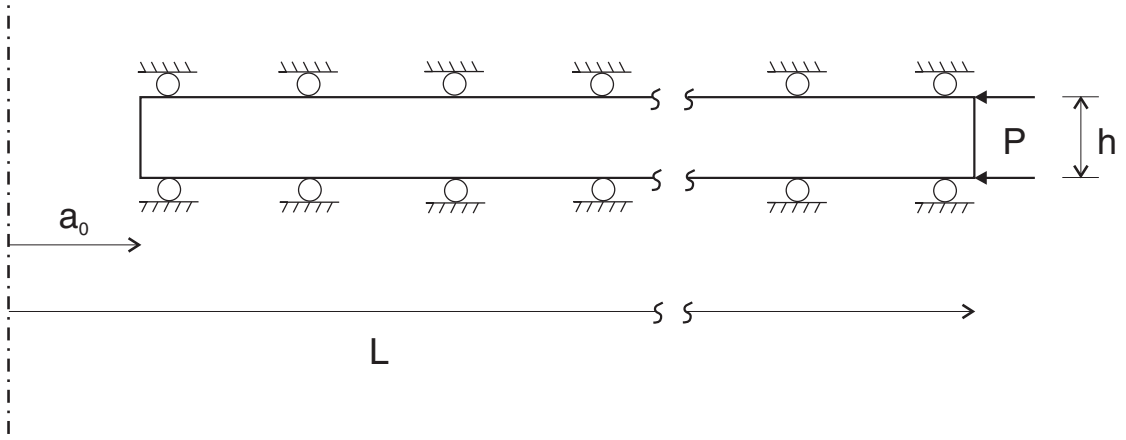

Figure 4.1 Model geometry

The dimensions of the *FLAC* grid correspond to dimensionless values $L/a_0 = 100$ and $h/a_0 = 1$, as indicated in Figure 4.2, where the *FLAC* system of reference axes is also represented. The grid is composed of a single layer of 31 zones of constant height and variable zone width, graded by a factor of 1.1.

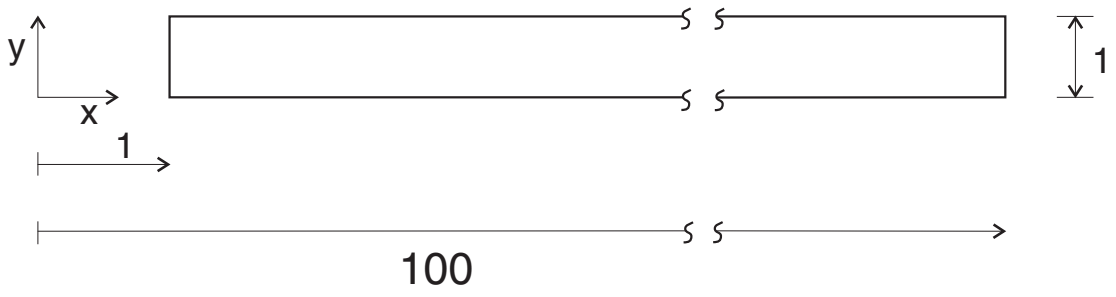

Figure 4.2 Grid geometry

Initially, the cavity boundary is fixed, in-situ stresses are installed, and a pressure boundary condition of magnitude $1.65C_u$ is applied at the far x-boundary. The groundwater configuration (**CONFIG gwflow**) is selected, and the no flow (**SET flow off**) and large-strain (**SET large**) options are specified.

The pre-consolidation pressure must be supplied to the numerical model. Since the soil is normally consolidated, this value is calculated from the given initial state. The corresponding values of mean pressure and deviator stress are $p'_0 = 2.1C_u$ and $q_0 = 1.35C_u$, and the pre-consolidation pressure, evaluated from the Cam-clay yield function (see Section 1.6.8 in **Constitutive Models**),

$$p'_{c0} = p'_0[1 + (q_0/(Mp'_0))^2] \tag{4.1}$$

is, hence, $2.70C_u$. The value of the over-consolidation ratio R, defined as $R = p'_{c0}/p'_0$, is approximately 1.29 for this problem.

As an illustration, initial values for the specific volume, v_0, and tangent bulk modulus, K_0, are specified. They correspond to the default values that would have been assigned by the code at the first step command:

$$v_0 = v_\lambda - \lambda \ln(p'_{c0}/p'_1) + \kappa \ln(p'_{c0}/p'_0) \tag{4.2}$$

$$K_0 = \frac{v_0 p'_0}{\kappa} \tag{4.3}$$

Here, information derived from v_0 and K_0 is used to specify the initial porosity, water and material bulk modulus.

The initial porosity is calculated from

$$n_0 = 1 - 1/v_0 \tag{4.4}$$

The bulk modulus of the water is set to 100 times the initial value of the product $K \times n$. This is sufficient to represent the water as incompressible relative to the clay. The maximum bulk modulus of the clay is set to 10 times the initial value.

A compressive velocity of magnitude $10^{-5}a_0$ is applied at the cavity boundary for a total of 100,000 steps to allow doubling of the cavity radius at the end of the pressure test. Stresses and pore pressure are monitored during the calculation.

The Cam-clay parameters are calculated in the *FISH* functions **set_prop** and **c_var**. The *FISH* function **b_table** creates tables to plot results for comparison to the solution by Carter et al. (1979).

4.3 Results and Discussion

The evolution of the deviator stress, q/C_u, at the cavity wall during the expansion is plotted in Figure 4.3. The numerical results indicate a failure level at $q/C_u = 1.778$. This value can be compared to the Cam-clay analytical prediction, as follows. Under undrained conditions, the yield path, followed by a normally consolidated stress point, has the form (see Section 15 in the **Verifications volume**)

$$\frac{p'_0}{p'} = \left(\frac{M^2 + \eta^2}{M^2 + \eta_0^2}\right)^{\Lambda} \tag{4.5}$$

where $\eta = q/p'$ and $\Lambda = (\lambda - \kappa)/\lambda$. The initial value $\eta_0 = q_0/p'_0$ can be derived from Eq. (4.1). Using the definition of R, we obtain

$$\eta_0^2 = RM^2 - M^2 \tag{4.6}$$

and the stress path becomes

$$\frac{p'_0}{p'} = \left(\frac{M^2 + \eta^2}{RM^2}\right)^{\Lambda} \tag{4.7}$$

Intersection of this stress path with the critical state line $q = Mp'$ or $\eta = M$ gives

$$q_{cr} = Mp'_0 \left[\frac{2}{R}\right]^{-\Lambda} \tag{4.8}$$

The prediction of q_{cr}/C_u derived from this formula is 1.771, a value in close agreement with that obtained numerically.

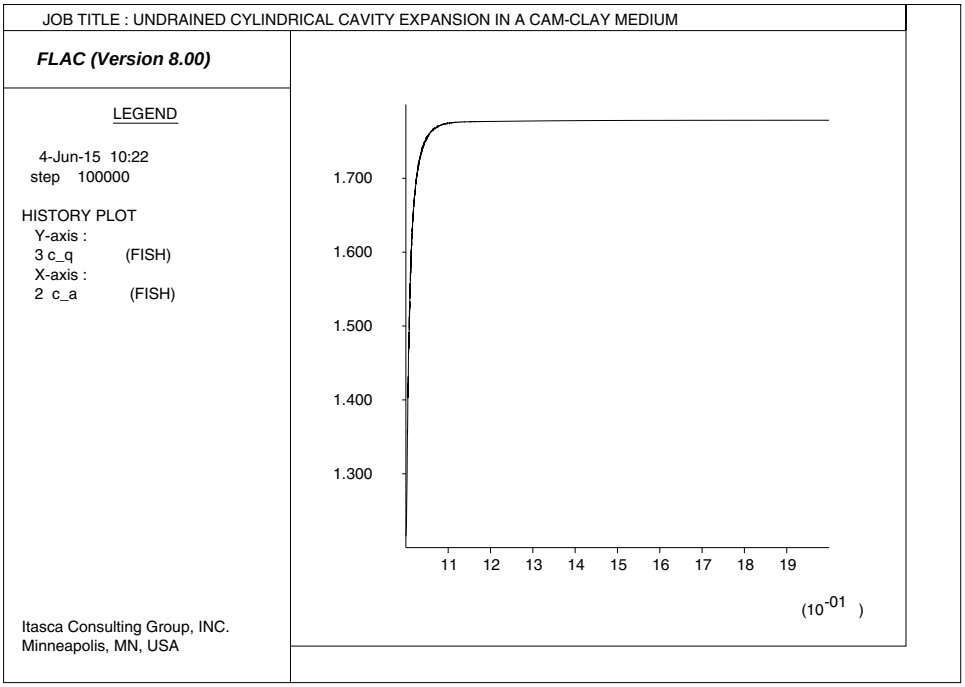

Figure 4.3 Deviator stress q/C_u at the cavity wall versus a/a_0

The variation of excess pore pressure and total radial stress at the cavity wall as the cavity expands is illustrated in Figure 4.4. These curves show a sharp rise followed by a gentle slope as pore pressure and radial stress approach a limit value.

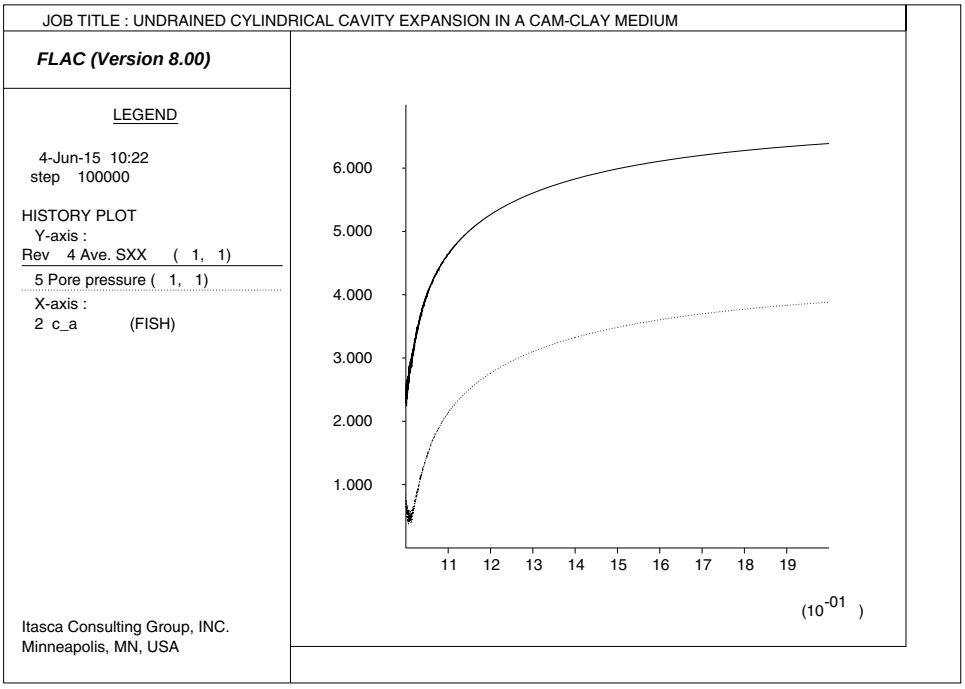

Figure 4.4 Total radial stress σ_r / C_u and excess pore pressure u_e / C_u at the cavity wall versus a/a_0

The radial distribution of effective stresses and pore pressure is plotted in Figure 4.5 when $a = 2a_0$. It may be seen that the stresses remain constant in an annulus around the cavity where the soil is at the critical state. There, the distribution of stresses has been greatly affected by the process of cavity expansion with radial and tangential stresses now in the role of minor and major principal stresses. The excess pore pressure develops mainly in this region. Further out, the stresses and pore pressure are shown to evolve towards their in-situ values. These results compare well with those presented by Carter et al. (1979).

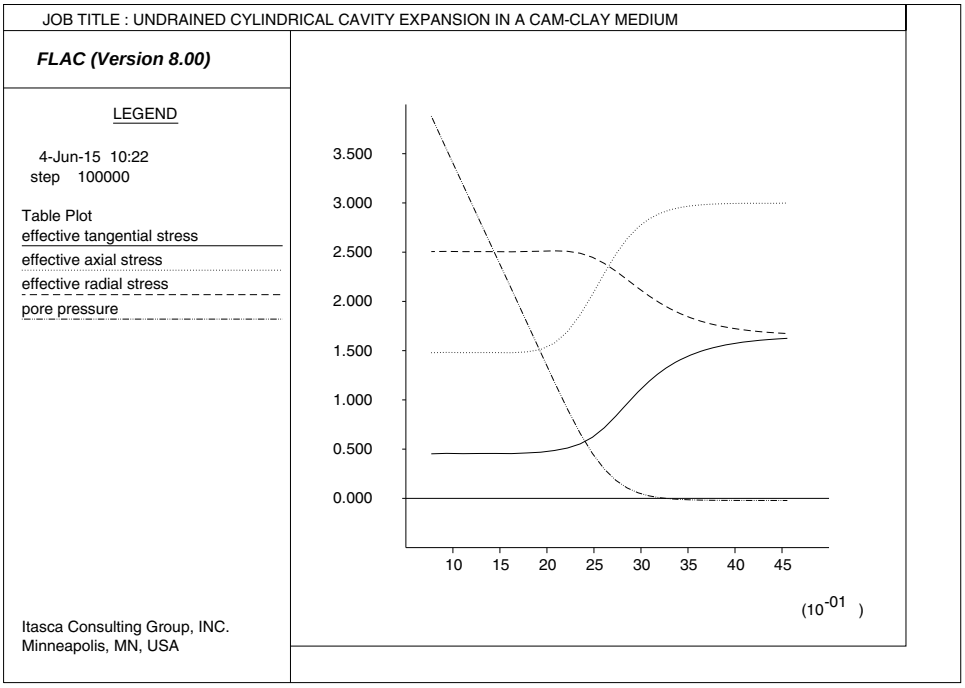

Figure 4.5 Radial distribution of effective stresses and pore pressure when $a = 2a_0$ ***plotted versus*** $ln(r/a_0)$

4.4 Reference

Carter, J. P., M. F. Randolph and C. P. Wroth. "Stress and Pore Pressure Changes in Clay during and after the Expansion of a Cylindrical Cavity," *International Journal for Numerical and Analytical Methods in Geomechanics*, ***3***, 305-322 (1979).